From the subtropics to the equator in the Southwest Pacific: Continental material fluxes quantified using neodymium data along modeled thermocline water pathways

M. Grenier, C. Jeandel, S. Cravatte

RESEARCH ARTICLE

Key Points:
- SW Pacific thermocline layers have contrasted pathways and geochemical evolutions
- The PNG margins and river discharges seem to play an important and complex role
- We present an original model-data coupling to quantify oceanic processes

Correspondence to:
M. Grenier,
melanie.grenier@utas.edu.au

From the subtropics to the equator in the Southwest Pacific: Continental material fluxes quantified using neodymium data along modeled thermocline water pathways

Mélanie Grenier[1,2], Catherine Jeandel[1], and Sophie Cravatte[1,3]

[1]LEGOS, Université de Toulouse, Centre National de la Recherche Scientifique, Centre National des Etudes Spatiales, Institut de Recherche pour le Développement, Toulouse, France, [2]Now at Antarctic Climate and Ecosystems CRC, IMAS Waterfront Building, Tasmania, Hobart, Australia, [3]IRD, Centre IRD de Nouméa, New Caledonia, Nouméa, France

Abstract The southwestern tropical Pacific, part of a major pathway for waters feeding the Equatorial Undercurrent, is a region of important geochemical enrichment through land-ocean boundary exchange. Here we develop an original method based on the coupling between dynamical modeling and geochemical tracer data to identify regions of enrichment along the water pathways from the subtropics to the equator, and to allow a refined quantification of continental material fluxes. Neodymium data are interpreted with the help of modeled Lagrangian trajectories of an Ocean General Circulation Model. We reveal that upper and lower thermocline waters have different pathways together with different geochemical evolutions. The upper thermocline waters entering the Solomon Sea mainly originate from the central subtropical gyre, enter the Coral Sea in the North Vanuatu Jet and likely receive radiogenic neodymium from the basaltic island margins encountered along their route. The lower thermocline waters entering the Solomon Sea mainly originate from northeast of New Zealand and enter the Coral Sea in the North Caledonian Jet. Depletion of their neodymium content likely occurs when flowing along the Australian and Papua coasts. Downstream from the Solomon Sea, waters flowing along the Papua New Guinea margins near the Sepik river mouth become surprisingly depleted in their neodymium content in the upper thermocline while enriched in the lower thermocline. This coupled approach is proposed as strong support to interpret the origin of the equatorial Pacific natural fertilization through a better understanding of the circulation, important objectives of the international GEOTRACES and SPICE programs, respectively.

1. Introduction

The equatorial Pacific thermocline is connected to the global ocean circulation through meridional cells which link the subtropical gyres to the Equatorial Undercurrent (EUC) via low latitude western boundary currents (LLWBCs). The physical and geochemical properties of the water masses constituting the thermocline are of prime importance because they directly influence those of the equatorial cold tongue [*Tsuchiya et al.*, 1989; *Rodgers et al.*, 2003], mostly its fertilization capacities [*Johnson et al.*, 1999; *Mackey et al.*, 2002; *Ryan et al.*, 2006]. The major contribution to the EUC comes from the southern LLWBCs (∼60%), beginning in the Coral and Solomon Seas and exiting through three narrow straits of the northern Solomon Sea [*Fine et al.*, 1994; *Blanke and Raynaud*, 1997; *Grenier et al.*, 2011] (see Figure 1 for the location of the seas, straits, and islands mentioned in the text). In these regions, the thermocline waters undergo significant geochemical enrichments: when flowing along Papua New Guinea margins [*Johnson et al.*, 1999; *Lacan and Jeandel*, 2001], identified as the major source of chemical enrichment of the equatorial thermocline waters, but also progressively from the Coral Sea to the Bismarck Sea [*Grenier et al.*, 2013].

Exchange processes between margin and water masses—"boundary exchange"—were suggested to be the enrichment mechanism [*Lacan and Jeandel*, 2005; *Grenier et al.*, 2013]. The boundary exchange concept relies on two mechanisms: (i) the supply of dissolved chemical elements through submarine weathering of sediment deposited on the margins, process that could modify the isotopic signature of the seawater if it differs from that of the source and (ii) the scavenging (i.e., removal from the seawater by adsorption on particles) of a fraction of these dissolved elements that occurs relatively shortly after the release, process that would not modify the seawater isotopic signature. The weathering process releases chemical elements to the ocean whereas the scavenging process is here defined as the net budget of particulate/dissolved
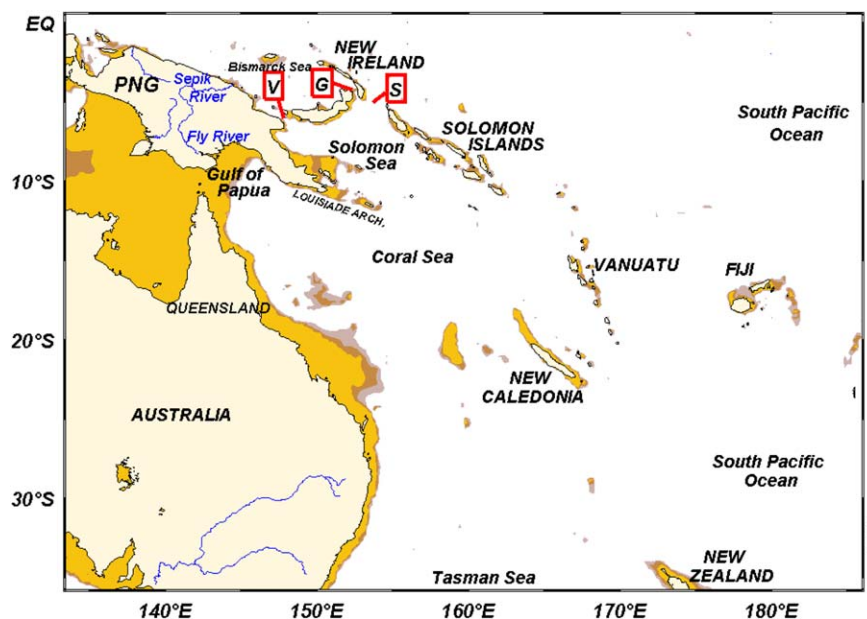
Figure 1. Reference map of the countries, seas, straits, and rivers mentioned in the text. PNG: Papua New Guinea. Red framed « V », « G », and « S », indicate Vitiaz Strait, St. George's Channel, and Solomon Strait, respectively. The bathymetry shallower than 100 m is colored in yellow, in brown if shallower than 250 m, and in light brown if shallower than 500 m.

exchanges and represents the removal of chemical elements from the dissolved phase. The net budget of boundary exchange (BE) is a net supply (positive value) when the release of dissolved element from margin sediments to seawater is larger than the removal of dissolved element from seawater to margin sediments; in the opposite case, the net BE is a net removal (negative value). Submarine weathering does not only release neodymium (Nd) but also micro and macronutrients, such as iron and silica, which impacts biological production [*Jeandel et al.*, 2011; *Jones et al.*, 2012; *Pearce et al.*, 2013]. Silicate weathering processes (aerial as submarine) consume CO_2 and therefore act as major CO_2 sinks. Furthermore, in the ocean, dissolved Si is an important limiting factor of the biological pump, another actor of CO_2 control, although on shorter time scales. Consequently, quantifying submarine weathering better is crucial to better constrain climate models [*Jeandel et al.*, 2011]. This is usually done with in situ geochemical data and coastal water transports deduced from the literature.

The aim of paper is to (1) refine the trajectories of waters in the South West Pacific, (2) characterize the evolution of the geochemical content of the thermocline waters in the southwestern tropical Pacific from their subduction zones to the Bismarck Sea, and (3) quantify boundary exchange (BE) fluxes occurring along their transits. In recent studies, upper and lower thermocline waters of the EUC were suspected to have different origins, pathways, and properties, based on their trace elements concentrations and on their signatures in Nd [*Slemons et al.*, 2010; *Grenier et al.*, 2013] and consistent with their distinct hydrological properties (salty and moderately oxygenated upper EUC waters, fresher but more oxygenated lower EUC waters) [*Tsuchiya et al.*, 1989; *Tomczak and Godfrey*, 2003; *Grenier et al.*, 2011]. This led us to distinguish these two layers in the present work. To achieve the quantification of BE fluxes, we use a novel coupled approach: following previous studies [*Lacan and Jeandel*, 2001, 2005; *Grenier et al.*, 2013], we use neodymium (Nd) data, tracers of continental sources (see section 2.2 for definition and details on Nd parameters). However, to better interpret measured Nd isotopic compositions (ICs) and concentrations—the real tracer—we also use a Lagrangian tool to quantify water transports simulated by high-resolution simulations of an Ocean General Circulation Model (OGCM)—the virtual tracer. This approach allows us to characterize the origins and pathways of the waters contributing to the Nd parameters sampled at one station. It also allows us to better estimate BE fluxes thanks to precise transports estimated from models. Boundary exchange (BE) estimation indeed depends on quantification of water transports, and the coarse estimation of water mass transports deduced from the literature in the previously published studies precluded a precise quantification of BE fluxes.

Although the lack of in situ data prevented a full application of the proposed approach, the present work demonstrates that coupling detailed circulation models to geochemical data is a key to provide reliable flux quantification in the ocean, one of the goals of the GEOTRACES program (http://www.geotraces.org). In addition, Lagrangian analysis applied to OGCM allows drawing refined circulation schemes and provides a good tool to adjust tracer's sampling strategy.

2. Tools and Experiment Definitions

2.1. The OGCM and the ARIANE Lagrangian Tool

Two different simulations were used to perform the Lagrangian experiments. The eddy-permitting $1/4°$ global OGCM ORCA025-G70 [*Barnier et al.*, 2006] was used for the large spatial scale study of the thermocline water circulation (see section 2.3). The eddy-resolving $1/12°$ regional fine-grid model, which extends from 143°E to 165°E and from 13°S to 0.5°S, was nested into a $1/4°$ regional model, itself nested into the global ORCA025-G70 we used for our study; these nesting processes ensure the consistency between the two models [*Melet et al.*, 2010]. This regional model was used for the study of the circulation within the key area of the Bismarck Sea. Its fine resolution allows a better reproduction of the bathymetry, of the coastlines and of the numerous straits of this complex area than in the $1/4°$ global model, which are crucial issues for a realistic representation of thermocline water pathways. The characteristics of the $1/4°$ global OGCM ORCA025-G70 [*Barnier et al.*, 2006] and of the $1/12°$ regional model were detailed in *Grenier et al.* [2011] and *Melet et al.* [2010], respectively. Both configurations are based on the ocean component of the Nucleus for European Modelling of the Ocean (NEMO) system, the Ocean Parallelisé (OPA) [*Barnier et al.*, 2006; *Madec*, 2008]. The vertical is composed of 46 geopotential levels, with spacing of 6 m near the surface, progressively increasing to 250 m at 5750 m, with partial steps at the bottom. This vertical resolution allows good resolution of the thermocline. Tracer diffusivity and momentum dissipation were performed isopycnally and along geopotential surfaces, respectively. Both were assigned a coefficient at the equator, decreasing poleward [*Melet et al.*, 2010]. Vertical mixing was computed using the turbulent kinetic energy (TKE) scheme of *Blanke and Delecluse* [1993].

Both models were initialized with the *Levitus et al.* [1998] temperature and salinity climatologies. The $1/4°$ global OGCM was forced over the 1958–2004 period with interannual varying forcing, whereas the $1/12°$ regional OGCM was integrated over the 1984–2004 period, with an initial period of 2 years used for the adjustment of the model. Surface wind stresses, precipitation, and radiation were provided by the Common Ocean-ice Reference Experiments data set (CORE) [*Yeager and Large*, 2004]. Because CORE used the ERA-40 data set over years 1958–2001 and ECMWF from 2002 to 2004, our Lagrangian analyses were performed over the 1971–2001 period for the $1/4°$ global OGCM and over the 1986–2001 period for the $1/12°$ regional OGCM to prevent adjustment of the model during the temporal integration.

The models were validated in the Solomon Sea and at the equator [*Melet et al.*, 2010, 2011; *Grenier et al.*, 2011] and their performances will not be shown in this study, for the sake of clarity and paper length. Here we first evaluated the $1/4°$ OGCM performance in the southwestern Pacific against the CARS climatology [*Ridgway et al.*, 2002] (Figures 2a and 2b). We plotted the mean salinity on two isopycnals corresponding to each thermocline water core (24.5 and 26.2 kg m^{-3}, respectively) with mean streamlines of geostrophic currents overlaid on each isopycnal surface [*Montgomery*, 1937]. For both isopycnal surfaces, the main circulation pathways are well represented in the model. Along 24.5 kg m^{-3}, the simulated salinity pattern is consistent with CARS climatology. The salty South Pacific Tropical Water (SPTW) outcrops in the high surface evaporation area (HSEA) and enters the Coral Sea north of 16°S (Figure 2) [*Kessler*, 1999]. However, in the model, the salinity was slightly overestimated and less eroded in the Coral and Solomon Seas than in CARS climatology. Along 26.2 kg m^{-3}, the two regions described by *Kessler and Cravatte* [2013]—salty Western South Pacific Central Water (WSPCW) and fresher Eastern South Pacific Central Water (ESPCW) with a front in the Coral Sea at 16°S—are well reproduced. Contrastingly to the upper layer, the modeled salinity was slightly underestimated and more eroded in the Coral and Solomon Seas than in CARS climatology. These biases may be due to an underestimated diapycnal mixing. However, they do not significantly impact the characteristics that we discuss in our study, since we are interested in pathways, not in water mass transformations.

We also compared the mean modeled and observed geostrophic North Caledonian Jet (NCJ) and North Vanuatu Jet (NVJ) along a vertical section west of New Caledonia (Figure 2c). For this purpose, we used the
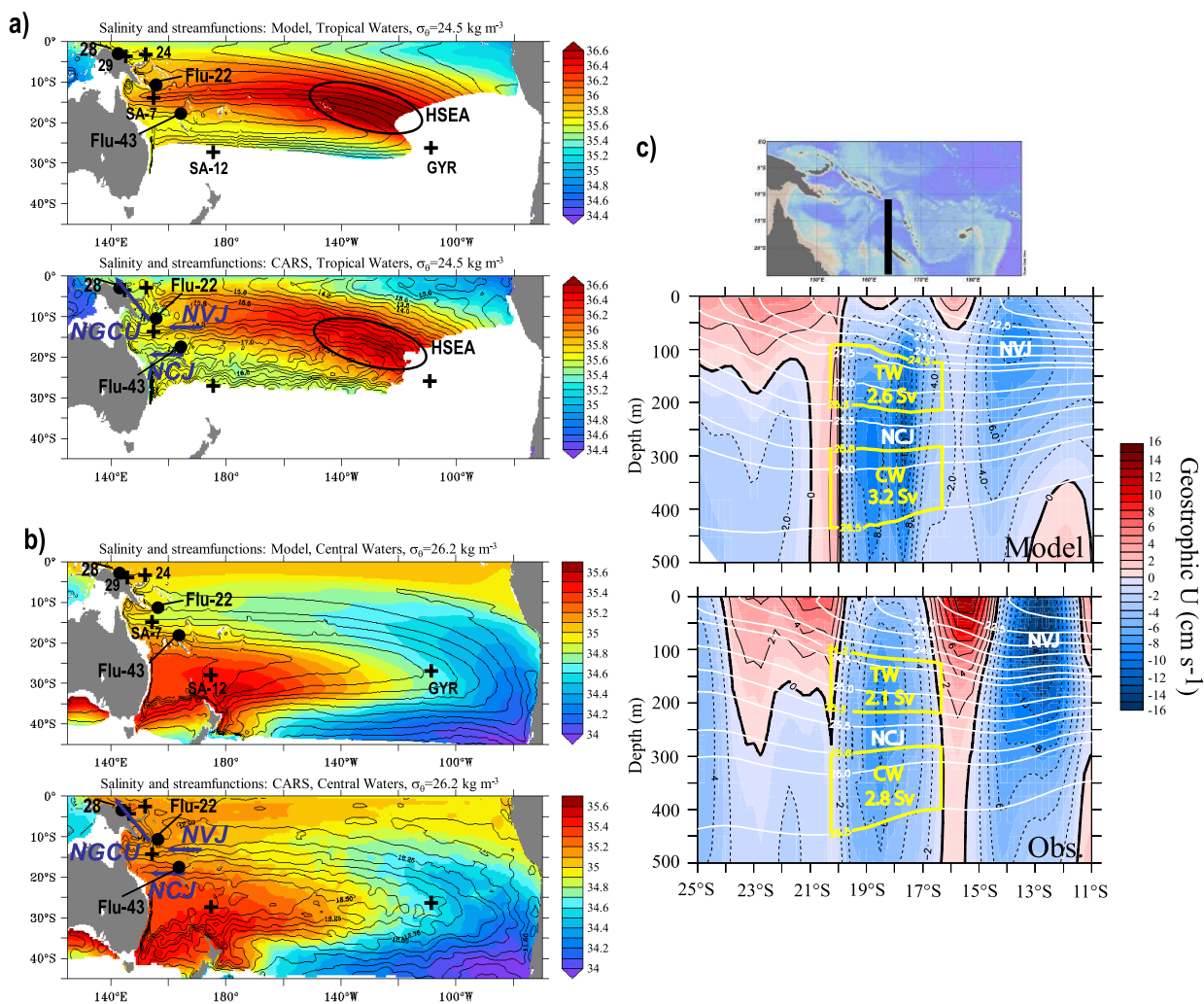
Figure 2. Mean salinity (colors) and geostrophic streamlines (contours) from (top) the model and from (bottom) the CARS climatology on the surfaces (a) 24.5 kg m^{-3} and (b) 26.2 kg m^{-3}. In both figures, overlaid contours show the geostrophic streamlines on the isopycnal relative to 2000 m, contoured every 0.2 Sv. The North Caledonian Jet (NCJ), North Vanuatu Jet (NVJ), and New Guinea Coastal Undercurrent (NGCU) are represented by blue arrows. The contoured area on the 24.5 kg m^{-3} isopycnal represents the High Surface Evaporation Area where the SPTW is outcropping (HSEA) [Grenier et al., 2013]. The black points and crosses represent stations where Nd data exist. The black points refer to the launching areas of the Lagrangian analysis: Flu-43, 163.68°E–17.53°S; Flu-22, 156.23°E–10.97°S; 28, 143.87°E–3.35°S. The Nd data obtained at black crosses are used in our study for the calculation of the exchange fluxes (see « Results » section): SA-7 and SA-12 [Zhang and Nozaki, 1996], GYR [Jeandel et al., 2013], 24, 29, and 30 [Grenier et al., 2013]. (c) Mean referenced zonal geostrophic currents (colors, in cm s^{-1}, contoured every 2 cm s^{-1}) across the averaged 163°E–164.5°E latitudinal section (see the map), from (top) the model (averaged between 1971 and 2001) and from (bottom) the ARGO/CARS merged product of Kessler and Cravatte [2013]. Red colors indicate eastward flow (U$_g$ > 0), blue westward (U$_g$ < 0). The NVJ and NCJ are identified. Mean isopycnals are shown in white contours. Yellow boxes illustrate the vertical section in the model where fluid particles are seeded for the Flu-43 Lagrangian experiment, for each thermocline layer (Tropical Waters, TW, and Central Waters, CW). Associated water mass transports are given (in Sv), for the model and for the observations.

observed absolute geostrophic current computed by Kessler and Cravatte [2013]. This Argo/CARS merged product is obtained from the CARS climatology hydrographic data (relative geostrophic velocities) referenced to a 1000 m velocity field derived from Argo float drift. In the first 500 m, the modeled NCJ is stronger and slightly narrower than the observed one. The water mass transports associated to the Tropical Water (TW) and Central Water (CW) layers in the yellow boxes, which correspond to the sections where we seeded particles in the Flu-43 Lagrangian experiments (see Figure 2c and section 2.3), reflect these differences, with slightly higher transports (15–20% higher) for both modeled TW (2.6 Sv) and CW (3.2 Sv) than observed (2.1 and 2.6 Sv, respectively). These results suggest that our model may slightly overestimate the transports of the TW and CW conveyed by the NCJ, although these differences could also partly be due to the inherent differences of data characteristics between the climatology of the Argo/CARS merged product and the average 1971–2001 of the model. The feature differences of the North Caledonian Jet between the model and

the observations are weak enough to allow us using our model with some confidence in the robustness of our water mass transport quantifications for the NCJ layers.

Contrastingly, the NVJ is weaker and larger in the model than in the observations. The NVJ water mass transport computed between 15.5°S and 11°S in the first 500 m is 8.8 Sv in the model and 12.0 Sv in the observations. This transport difference mainly stems from the lower part of the NVJ, below 200 m, where the observed NVJ becomes larger. Indeed, within the isopycnal ranges we used for the definition of the Tropical Waters and Central Waters (24.3–25.3 and 25.8–26.5 kg m^{-3}, respectively; see section 2.3), we found a transport of 2.3 Sv for the modeled TW and 2.4 Sv for the observed TW. By contrast, we found a transport of only 1.4 Sv for the modeled CW while we calculated 2.3 Sv for the observed one. Consequently, the modeled NVJ contribution may be underestimated in the backward Flu-22 CW experiment. Thus, we will be cautious concerning the quantification of the geochemical fluxes for this experiment, in the result discussion.

To conclude, the agreement between our simulation and observations in terms of circulation and of saline distribution for each thermocline layer allows us to analyze the thermocline water mass pathways and transports in the southwestern Tropical Pacific using our model with some confidence in the robustness of our results.

The Lagrangian analysis (ARIANE algorithm, http://stockage.univ-brest.fr/~grima/Ariane/) [*Blanke and Raynaud*, 1997; *Blanke et al.*, 1999] is a powerful tool to diagnose the origin and fate of water masses [*Grenier et al.*, 2011; *Melet et al.*, 2011; *Rodgers et al.*, 2003]. In brief, this off-line diagnostic tool temporally integrates the 5 day (daily) average velocity fields modeled by the $\frac{1}{4}°$ global OGCM ($\frac{1}{12}°$ regional OGCM) to compute the mean 3-D streamfunctions of water masses. It only uses advection to trace the streamlines of the injected fluid particles, the diffusion being implicitly resolved by the along-trajectory changes in T-S properties [*Blanke et al.*, 1999]. At injection segments, particles are seeded at each time step of the model, bearing an infinitesimal transport; the sum of all the transports amounts to the available inflow. The temporal integration was led backward in time to analyze water mass sources and their subduction areas.

2.2. Nd Isotopic and Concentration Parameters

Nd in the ocean is mainly of terrestrial origin. The Nd isotopic compositions (IC) of continental rocks vary as a function of their chemical composition and age. This chemical element is brought to the ocean through rivers, atmospheric dust, boundary exchange, and hydrothermal vents, which tag the seawater with the Nd IC associated to the nearby supply of continental material [*Piepgras and Wasserburg*, 1987; *Lacan and Jeandel*, 2005; *Singh et al.*, 2012]. The Nd IC of any water mass varies whether it mixes with a water mass characterized by a different Nd IC or whether a supply of continental material of different Nd IC occurs. The Nd IC is expressed as:

$$\varepsilon_{Nd} = \left(\frac{\left(^{143}Nd/^{144}Nd\right)_{sample}}{\left(^{143}Nd/^{144}Nd\right)_{CHUR}} - 1 \right) * 10^4$$

where CHUR stands for Chondritic Uniform Reservoir and is a reference value representing the average earth isotopic composition, presently 0.512638 [*Wasserburg et al.*, 1981].

Along its pathway, the Nd concentration of any water mass increases or decreases, respectively, depending on whether fluxes of supply or scavenging of Nd dominate. In case of equivalent supply and scavenging fluxes, the Nd concentration of the water mass remains constant, concealing signs of exchange processes. Contrastingly, the water mass is tagged by different signatures of ε_{Nd} involved in the mixing or supply processes, recording signs of exchanges. Thus, coupling the Nd parameters of a water mass allows quantifying supply fluxes (imprinted in ε_{Nd} changes) and scavenging fluxes (imprinted in Nd concentration changes) occurring along the water mass pathway. Realistic pathways and water mass transport quantifications are necessary to get realistic flux calculations.

Here we determine the origins of waters flowing through three locations identified by black points in Figure 2 (in the North Caledonian Jet, at the entrance of the Solomon Sea, and downstream from the Sepik River). Black points and crosses identify stations where Nd data are available [*Grenier et al.*, 2013]. These data will constrain exchange flux calculations (see section 3). Stations sampled in the Coral and Solomon Seas were occupied during the FLUSEC-01 cruise (stations Flu-22 and Flu-43; August 2007) [*Gasparin et al.*, 2012]. At these two stations, no water was sampled in the density range (25.8–26.5) kg m^{-3} that we defined for the Central Waters (CW) [see *Grenier et al.*, 2013, Table 1]. Therefore, here we considered the Nd IC of slightly shallower water samples ($\sigma_\theta = 25.5$ kg m^{-3} at Flu-43 and $\sigma_\theta = 25.6$ kg m^{-3} at Flu-22) for the geochemical

Table 1. Absolute (Sv) and Relative (%) Transports Obtained for the Six Lagrangian Experiments

		1° BACKWARD FLU-43 TW		2° BACKWARD FLU-43 CW	
Injection criterion		$24.3 \leq \sigma \leq 25.3$		$25.8 \leq \sigma \leq 26.5$	
Interception criterion		Mixed layer OR t > 30 years: 100%; 0%		Mixed layer OR t > 30 years: 65%; 35%	
	Interception criterion	**2.5**	87%	**3.1**	79%
	Meanders	0.2	7%	0.4	9%
SECTIONS	SE Flu-43	0.2	6%	0.3	7%
	NE 140° W			0.1	3%
	SE 140° W			0.1	2%
	TOTAL	**2.9**		**3.9**	
		3° BACKWARD FLU-22 TW		4° BACKWARD FLU-22 CW	
Injection criterion		$24.3 \leq \sigma \leq 25.3$		$25.8 \leq \sigma \leq 26.5$	
Interception criterion		Mixed layer OR t > 30 years: 100%; 0%		Mixed layer OR t > 30 years: 89%; **11%**	
	Interception criterion	**1.8**	**52%**	**1.1**	**23%**
	Flu-43	**0.8**	**24%**	**2.0**	**42%**
SECTIONS	Meanders	**0.7**	**22%**	**0.8**	**17%**
	NE 140° W			**0.5**	**11%**
	SE 140° W			0.2	5%
	TOTAL	**3.4**		**4.7**	
		5° BACKWARD 28 TW		6° BACKWARD 28 CW	
Injection criterion		$24.3 \leq \sigma \leq 25.3$		$25.8 \leq \sigma \leq 26.5$	
Interception criterion		Mixed layer OR t > 5 years: 100%; 0%		Mixed layer OR t > 5 years: 73%; 27%	
	30	**2.0**	75%	**3.4**	77%
SECTIONS	St Georges	**0.3**	**11%**	**0.6**	**13%**
	24	**0.3**	**10%**	0.3	6%
	TOTAL	**2.6**		**4.4**	

[a]Only sources whose contribution is greater than 2% are reported, in bold if greater than 10%. The sources are defined as the different colored sections delimiting the boxes in Figures 3 and 4. The « injection criterion » specifies the density range within which particles were injected. A particle is stopped by one of the section or when it encounters the mixed layer (defined as $\sigma_\theta - \sigma_o \leq 0.01$ kg m^{-3} and counted in the « Interception criterion »). If the particle did not reach a section within the time limit allowed, it is also counted in the « Interception criterion ». The percentages detailed in the « Interception criterion » line correspond to the mixed layer interception (that is 100%, for instance, for experiment 1°) relative to the temporal interception (that is 0%, for instance, for experiment 1 °).

flux calculations of the CW layer. Furthermore, Nd concentrations of the thermocline waters are not available at Flu-43 and Flu-22, thus we estimated the Nd concentrations of Flu-22 and Flu-43 waters from the concentrations of the Tropical Waters (TW) and Central Waters (CW) proposed by *Zhang and Nozaki* [1996], collected at stations SA-7 and SA-12, respectively. Seawater samples north of the Solomon Sea were collected during the EUC-Fe cruise (stations 24, 28, and 29; September 2006) [*Slemons et al.*, 2010]. Analytical procedures yielding the isotopic and concentration analyses of these samples are detailed in *Grenier et al.* [2013]. Similar to stations Flu-22 and Flu-43, Nd concentrations of the thermocline waters collected at station 29 are not available and were estimated from those measured by *Zhang and Nozaki* [1996] at station SA-7. The station GYR was occupied during the BIOSOPE cruise (December 2004) [*Jeandel et al.*, 2013]. Nd ICs and concentrations used in this study to characterize the thermocline waters of this station stem from *Jeandel et al.* [2013]. The CW were associated to the Nd IC of a slightly shallower water sample ($\sigma_\theta = 25.4$ kg m^{-3}) at this station GYR, which allows a consistent quantification of the CW geochemical fluxes between this station and the Flu-43 and Flu-22 stations.

2.3. Definition of the Lagrangian Experiments

The Lagrangian experiments, performed in quantitative mode, were defined in order to quantify the transports by the upper and lower thermocline between the geochemical stations referred to as black points and crosses in Figures 3 and 4. Here we focused on the transport distribution upstream and downstream of the Solomon Sea, which complements previous studies [*Rodgers et al.*, 2003; *Melet et al.*, 2010; *Grenier et al.*, 2011].

Four backward experiments were conducted with the $1/4°$ global OGCM, between the Solomon Sea and the subtropics, and two with the $1/12°$ regional OGCM, in the Bismarck Sea. Two experiments investigated the sources of the Tropical Waters (TW) and Central Waters (CW) entering the Coral Sea south of Vanuatu,
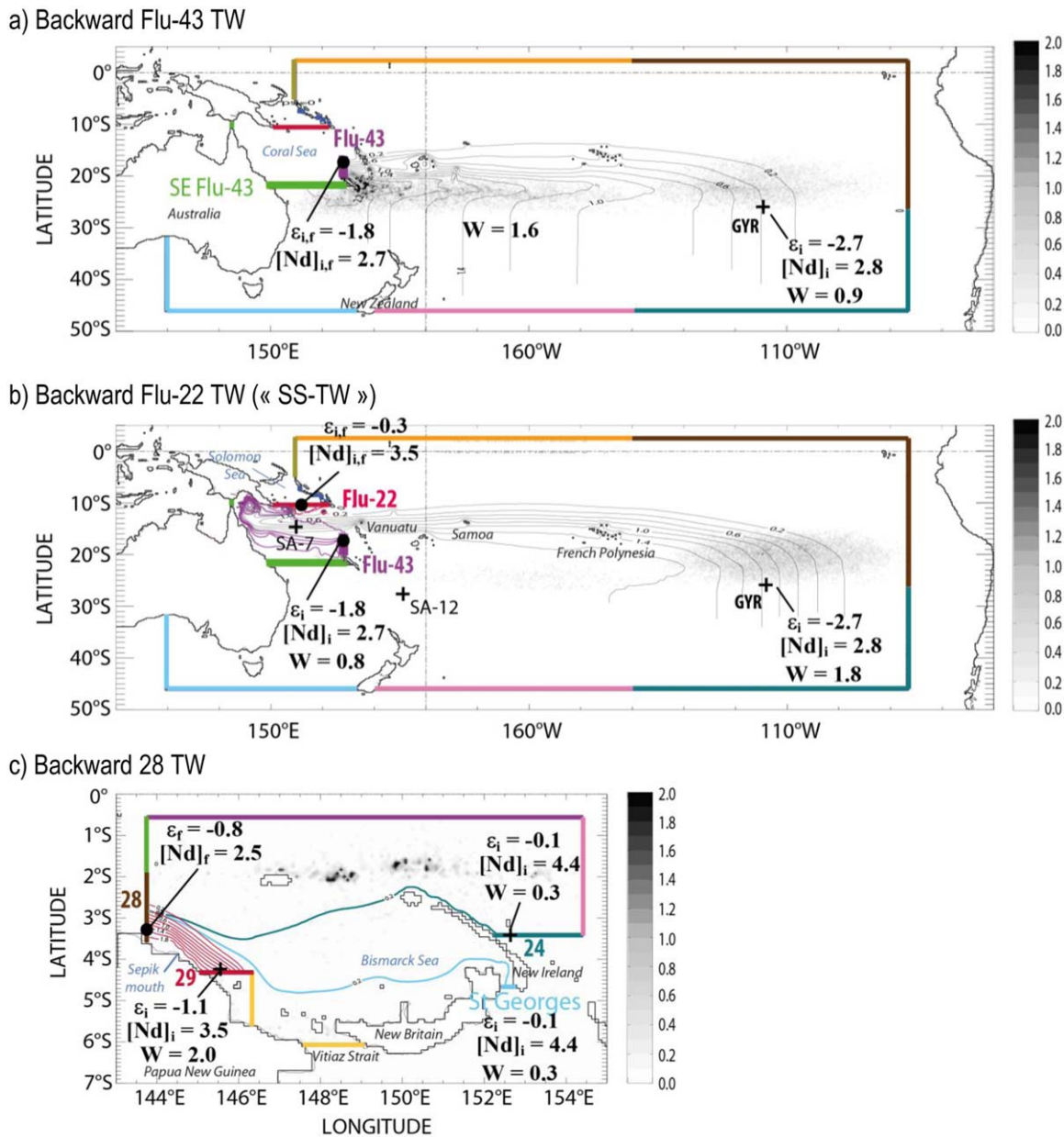
Figure 3. Mean streamfunctions of the TW, contoured every 0.2 Sv, given by the backward experiments for (a) Flu-43, (b) Flu-22, and (c) EUC-Fe 28. The colored sections delimit the box within which the particles are traced. The color of the streamline refers to the interception section. The gray patches represent the mixed layer interception, whose intensity is given by the associated gray scale bar (in 10^{-4} Sv). The black points refer to the geochemical stations identified in Figure 2. The geochemical data (ε, dimensionless and [Nd], in pmol kg^{-1}) and transports (W, in Sv) used for the calculation of the boundary exchange flux are reported for each major contributor. Nd concentrations of stations Flu-22 and Flu-43 were estimated from the data of SA-7 and SA-12 stations, respectively [*Zhang and Nozaki*, 1996].

conveyed by the North Caledonian Jet (NCJ) and are associated with the geochemical station Flu-43 (Figures 2, 3a, and 4a). Two others identified the sources of the TW and CW entering the Solomon Sea and are associated to the geochemical station Flu-22 (Figures 2, 3b, and 4b). The last two illustrated the pathways of the TW and CW flowing along the Papua New Guinea coast downstream Vitiaz Strait, and are associated with the geochemical station 28 (Figures 2, 3c, and 4c). For each experiment, particles were initially injected at one station within a specific density range specified in Table 1 as "injection criterion." The density ranges were defined following the density layers of the upper and lower thermocline waters of the Equatorial Undercurrent (EUC). Thus, for the experiments investigating the TW, particles were initially injected within the density range $\sigma_\theta = (24.3–25.3)$ kg m^{-3} while for the experiments investigating the CW they were initially injected within the density range $\sigma_\theta = (25.8–26.5)$ kg m^{-3}. These particles were integrated backward in time until they reached
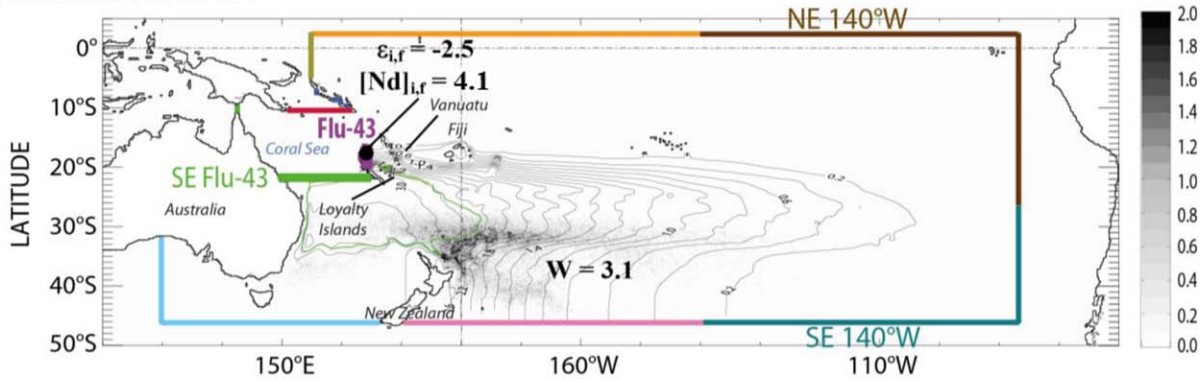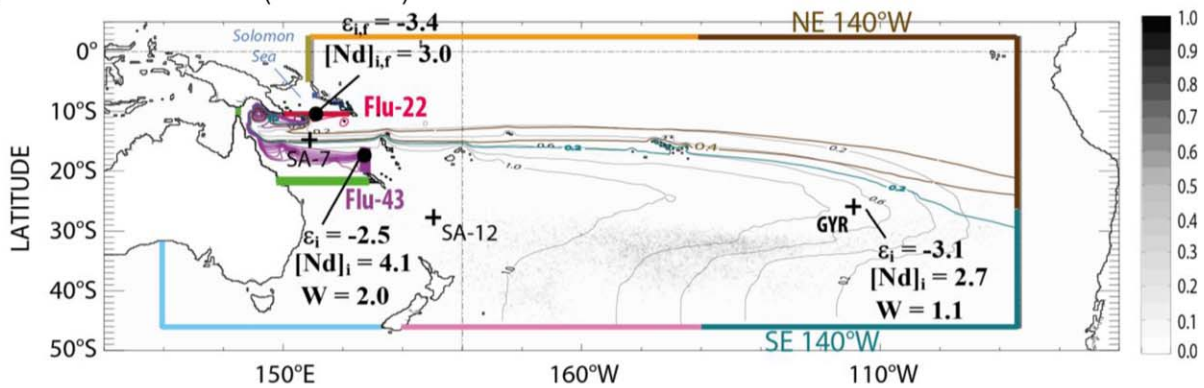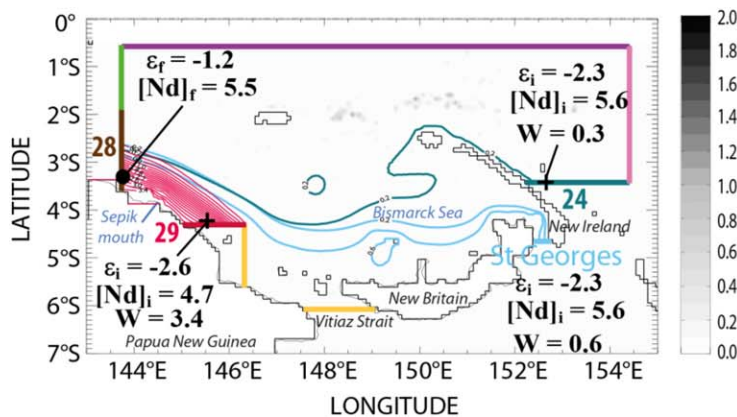
Figure 4. As Figure 3, for the CW.

the base of the mixed layer (to deduce their subduction zone) or one of the "sections" defined in Table 1. The integration was performed over a sufficiently long period of time, varying from 5 years for the Bismarck Sea experiments to 30 years for the longest ones (see Table 1), in order to be sure that a maximum of particles were intercepted by a section or by the mixed layer before the end of the integration time. The "interception criterion," which refers to the temporal and/or mixed layer interception, is given in Table 1.

3. Results

3.1. Water Mass Pathways and Transports

As shown by previous observations, thermocline waters enter the Coral Sea via two strong westward currents located north and south of Vanuatu: the North Vanuatu Jet and the North Caledonian Jet [*Qu and*

Lindstrom, 2002; *Gourdeau et al.*, 2008; *Gasparin et al.*, 2011]. The North Caledonian Jet (NCJ) and part of the North Vanuatu Jet (NVJ) convey thermocline waters toward the Australian coast and bifurcate equatorward and poleward. The northern branch flows past the coasts of Queensland and Papua New Guinea to form the Gulf of Papua Current (GPC) [*SPICE Community*, 2012]. Before entering the Solomon Sea, southeast of the Louisiade Archipelago (locations are referenced in Figure 1), the GPC mixes with the second branch of the North Vanuatu Jet that retroflects northward south of the Solomon Sea entrance without reaching the Gulf of Papua to form the NGCU [*Kessler and Cravatte*, 2013]. Here we propose to (i) characterize the subduction areas of these waters and their pathways to the Coral Sea and (ii) quantify the transport of each source contributing to the formation of the thermocline waters in the Coral, Solomon, and Bismarck Seas.

The water mass pathways obtained from the Lagrangian experiments are illustrated by the mean streamfunctions in Figures 3 and 4; the main transports are summed up in Table 1. The modeled pathways in the Coral Sea agree well with the circulation described above, strengthening our confidence in the pathways, transports, and outcropping areas simulated by the Lagrangian analyses.

The modeled Tropical Waters entering the Coral Sea in the North Caledonian Jet (NCJ-TW) originally subducted between 20°S and 25°S, slightly further north than *Qu and Lindstrom*'s [2002] suggestions, in two different regions (gray patches and thin black streamfunctions in Figure 3a). About 40% (0.9 Sv) subducted east of 140°W in the vicinity of station GYR, in the area of high surface evaporation (Figure 2). Surprisingly, ∼60% (1.6 Sv) subducted west of 140°W mainly south and southeast of New Caledonia. Both TW turn westward around 23°S toward the Coral Sea. The backward experiment from station Flu-22 located at the entrance of the Solomon Sea reveals that part of the NCJ-TW bifurcates northward and mixes with Tropical Water conveyed by the North Vanuatu Jet (NVJ-TW; Figure 3b) in the proportions of ∼25% (0.8 Sv) and ∼50% (1.8 Sv), respectively, before entering the Solomon Sea (Table 1). The remaining fraction of TW entering the Solomon Sea (25%) is mainly associated with recirculation in the eastern part of the Solomon Sea [*Gasparin et al.*, 2012]. In the following, this mixture of TW will be called the Solomon Sea Tropical Water (SS-TW). TW entering the Solomon Sea that flowed upstream in the North Vanuatu Jet originally subducted in the high salinity evaporation area, slightly northeast of station GYR, in agreement with *Tomczak and Hao* [1989] (gray patches and thin black streamfunctions in Figure 3b). Downstream of the Solomon Sea, the modeled TW flowing along the Papua New Guinea coast up to 3°S (station 28) mainly exited the Solomon Sea via the NGCU through Vitiaz Strait (not shown), as suggested by *Tsuchiya et al.* [1989], *Melet et al.* [2010], and *Grenier et al.* [2011], then flowing past the coast at the location of station 29 (2.0 Sv—75%). Only 10% originated from Solomon Strait (station 24) and St. George's Channel (Table 1 and Figure 3c).

Pathways of the underlying denser Central Waters are somewhat different. Those entering the Coral Sea in the North Caledonian Jet (NCJ-CW) are mostly traced backward along an anticyclonic loop to their outcropping area northeast of New Zealand (3.1 Sv; 79%; gray patches and thin black streamfunctions in Figure 4a), in agreement with *Tsuchiya* [1981], *Roemmich and Cornuelle* [1992], and *Qu et al.* [2009]. The remaining flow recirculates around New Caledonia, as shown by the green line in Figure 4a. The backward experiment from station Flu-22 located at the entrance of the Solomon Sea shows that part of this NCJ-CW bifurcates northward to the Solomon Sea and mixes at its southern entrance with Central Water conveyed by the North Vanuatu Jet (NVJ-CW; Figure 4b), in the following proportions: 42% (2.0 Sv) are NCJ-CW (station Flu-43), 23% (1.1 Sv) are NVJ-CW, and 17% (0.8 Sv) are recirculating in the eastern part of the Solomon Sea (Table 1 and Figure 4b). In the following, this mixture of CW will be called the Solomon Sea Central Water (SS-CW). The absolute contribution of the NVJ-CW within the SS-CW may be underestimated, due to the underestimation of the NVJ in the model, below 200 m depth, as discussed in section 2.1 (Figure 2c). The NVJ-CW are traced backward along a wide anticyclonic loop to their subduction area southwest of station GYR, in the vicinity of 140°W–33°S (gray patches and thin black streamfunctions in Figure 4b). During their transit in the gyre, they flow close to the location of station GYR. Finally, the modeled CW flowing along the Papua New Guinea coast up to 3°S mainly flow upstream at station 29 (3.4 Sv; 77%), after having exited the Solomon Sea via the NGCU through Vitiaz Strait (not shown). Among the remaining 20%, 2/3 may exit the Solomon Sea by St. George's Channel and 1/3 by Solomon Strait (station 24; Figure 4c).

3.2. Neodymium Exchange Fluxes Between Continental Margins and Water Masses
Observed enrichments of the EUC in geochemical elements (micronutrients, Nd isotopes) are attributed to the heavily sediment-loaded runoff of the PNG and neighbour islands [*Johnson et al.*, 1999; *Lacan and*

Jeandel, 2001; *Mackey et al.*, 2002]. *Lacan and Jeandel* [2001] proposed a first estimate of the exchanged fluxes between water masses and margins using a simple box model describing the input and output fluxes of Nd parameters in the surface and intermediate waters flowing along Vitiaz Strait (Figure 5a) [*Lacan and Jeandel*, 2001, 2005]. The large scale of the considered area (comprised between 140°W and the PNG coast) constrained them to hypothesize a rough circulation scheme, while it is known as very complex. Moreover, the regional approach prevented these authors to precisely locate where and at which rate the enrichments were occurring. Among others, they could not identify how these enrichments affect the different isopycnal levels involved in the trajectories. Because water transports are deduced from realistic and high-resolution OGCM simulations, the parameters of the box model proposed here are better constrained than in the former study. This model calculates the fluxes required to balance Nd concentrations and isotopic compositions (ICs) between the incoming and outgoing water masses, assuming only isopycnal mixing (Figure 5a). These calculated fluxes are the flux of dissolved Nd imported from the margins to the water mass ($F_{ex,tot}$) and the flux of dissolved Nd exported from the water mass toward the sediments due to adsorption of dissolved Nd on the particles, a process called "scavenging" ($F_{sc,tot}$). When two different sources are feeding the water that exits the box (as illustrated in Figure 5a), the required parameters to perform the model calculation are: the modeled source transports W and W', the initial and final Nd concentrations, and ε_{Nd} of the water masses ($[Nd]_i$, $[Nd]_i'$, and $[Nd]_f$ and ε_i, ε_i', and ε_f, respectively), the isotopic composition of the external fluxes, which are the margins encountered along the two pathways of the sources (ε_{ex} and ε_{ex}'), and the isotopic compositions of scavenging fluxes (ε_{sc} and ε_{sc}'), that are included in the variation range of the water mass isotopic composition $[\varepsilon_i, \varepsilon_f]$. Assuming steady state and mass conservation, we obtain the following equations:

$$(W+W').[Nd]_f = W.[Nd]_i + W'.[Nd]_i' + F_{net,tot} \qquad (1)$$

$$(W+W').\varepsilon_f.[Nd]_f = W.\varepsilon_i.[Nd]_i + W'.\varepsilon_i'.[Nd]_i' + F_{ex}.\varepsilon_{ex} + F_{ex}'.\varepsilon_{ex}' - F_{sc}.\varepsilon_{sc} - F_{sc}'.\varepsilon_{sc}' \qquad (2)$$

where $F_{net,tot} = F_{ex,tot} - F_{sc,tot}$, $F_{ex,tot} = F_{ex} + F_{ex}'$, and $F_{sc,tot} = F_{sc} + F_{sc}'$.

We used this box model to estimate the geochemical fluxes received by the waters entering the Solomon Sea, along their pathways from the southeastern Pacific—GYR station—and from north of New Caledonia—Flu-43 station—(backward experiments from Flu-22 station: Figures 3b and 4b). We were also able to quantify the geochemical fluxes received by the thermocline waters in the Bismarck Sea along the PNG coast (backward experiments from station 28: Figures 3c and 4c). However, the lack of published Nd data in the subduction areas of NCJ-TW and NCJ-CW (Figures 3a and 4a) prevented us from estimating the geochemical fluxes obtained upstream by waters flowing in the North Caledonian Jet.

3.2.1. Total Net Fluxes
Equation (1) allowed us to determine the total net flux $F_{net,tot}$ for each experiment. These net fluxes $F_{net,tot}$ are reported in Figure 5b; their sign indicates which flux (input or scavenging) is dominant along the pathways of the different thermocline waters. The error bars were calculated by the statistic formula of error propagation.

External Nd inputs clearly dominate Nd scavenging along the transit of the SS-TW before entering the Solomon Sea ($F_{net,tot} = +1.9 \pm 0.2$ t(Nd) yr^{-1}; Figure 3b). Contrastingly, scavenging of dissolved Nd prevails over PNG margin inputs along the pathways followed by the TW along the PNG coast in the Bismarck Sea ($F_{net,tot} = -3.0 \pm 0.4$ t(Nd) yr^{-1}; Figure 3c). At these densities, waters are enriched in Nd along their transit in the southwestern Pacific before their entrance in the Solomon Sea, and then depleted in Nd content along the PNG coast.

Surprisingly, only ~100 m deeper, within the Central Waters, these tendencies are reversed (Figure 4). Central waters are depleted from their Nd content along their transit in the South West Pacific before their entrance in the Solomon Sea, and enriched in Nd along the PNG coast. The negative F_{net} calculated for the SS-CW suggests that a scavenging of dissolved Nd onto marine particles dominates ($F_{net,tot} = -1.6 \pm 0.5$ t(Nd) yr^{-1}; Figure 4b). The Nd concentration decrease between the entrance of the Coral Sea (Flu-43) and the entrance of the Solomon Sea (Flu-22) implicitly suggests that scavenging is particularly strong during the NCJ-CW transit along the Australian and Papua coasts (purple streamfunctions in Figure 4b). However, the underestimation of the modeled NVJ transport in the CW layer could suggest an underestimation of the
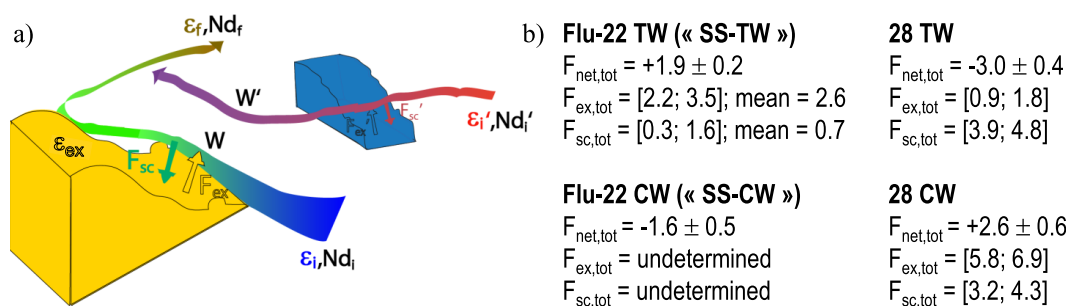
Figure 5. (a) Schematic description of the boundary exchange principle. It illustrates the Nd evolution of a water mass along its transit, initially characterized by an isotopic composition (IC) ε_i and a concentration Nd_i. Each arrow represents a water mass and the color code refers to the IC of each element (margin or water mass). In the box model, two processes can change these initial Nd parameters ε_i (blue) and Nd_i: (i) boundary exchange with a continental margin characterized by a different IC ε_{ex}, (yellow), (ii) mixing with a water mass characterized by different Nd parameters, $\varepsilon_i{}'$ (red) and $[Nd]_i{}'$. The boundary exchange is defined by two fluxes: the Nd flux supplied by the margin F_{ex}, that modifies the IC of the water mass (green), and the Nd flux removed from the water mass toward the sediment F_{sc} that balances the concentration budget. The total net flux is defined as $F_{net,tot} = F_{ex,tot} - F_{sc,tot} = F_{ex} + F_{ex}{}' - F_{sc} - F_{sc}{}'$. W and W′ are the transport of the water masses determined by the Lagrangian analysis. The output values of the box model refer to the resulting water mass Nd parameters, ε_f (brown) and Nd_f. (b) Total net fluxes $F_{net,tot}$ calculated from equation (1) and ranges and mean values of $F_{ex,tot}$ and $F_{sc,tot}$ calculated according to the different hypotheses (detailed in section 3.2.2 for station 28 and in the Appendix A for station Flu-22), for each studied water mass (in tons of Nd per year). The estimations of the exchange fluxes occurring along the Flu-22 CW are not reported because they were too variable, precluding us from suggesting a likeable estimation.

scavenging fluxes along the NCJ-CW pathway. Contrastingly, external inputs of Nd dominate its removal by scavenging as the CW flow along the coasts of PNG and New Ireland ($F_{net,tot} = +2.6 \pm 0.6$ t(Nd) yr^{-1}; Figure 4c). It is interesting to note that for both thermocline levels, the net fluxes are larger for the water masses flowing downstream from the Solomon Sea, along the PNG coast. The enrichment/depletion processes revealed here and that are oppositely affecting TW and CW could not have been evidenced by the study of *Lacan and Jeandel* [2001], conducted on a too large scale.

3.2.2. Total Supply and Scavenging Fluxes Quantified for Water Masses Flowing Along the PNG Coasts (28 TW and 28 CW Experiments)

To go further, we estimated the values of scavenging and input fluxes along the pathways of the waters flowing along the PNG coast at station 28. Equation (2) has four unknowns (F_{ex}, $F_{ex}{}'$, F_{sc}, and $F_{sc}{}'$) that cannot be determined using only two equations without making assumptions. For the 28 TW and 28 CW experiments, we first considered only the pathway that comes from station 29. Indeed the Lagrangian experiments showed that the major part of the transport constituting the upper and lower thermocline waters of station 28 followed this pathway (Table 1 and red streamfunctions of Figures 3c and 4c). From this assumption, we quantified F_{ex} and F_{sc} and, with those values fixed, we were then able to quantify the likely $F_{ex}{}'$ and $F_{sc}{}'$ associated with the minor pathways (blue and green streamfunctions of Figures 3c and 4c).

The isotopic signature of the PNG margin—ε_{ex}—was determined from measurements on bottom sediment samples collected in the Bismarck Sea, between stations 28 and 29 ($\varepsilon_{ex} = +2.8$). We calculated the fluxes $F_{ex,tot}$ and $F_{sc,tot}$ in two ways: (i) assigning ε_{sc} to ε_i; (ii) assigning ε_{sc} to ε_f. This choice is justified in the paragraph 1.1 of Appendix A. We obtained two values for each flux, one when considering $\varepsilon_{sc} = \varepsilon_i$ and another when considering $\varepsilon_{sc} = \varepsilon_f$, and we finally expressed the fluxes $F_{ex,tot}$ and $F_{sc,tot}$ as ranges of values between these two values. They are reported in Figure 5b.

For the TW flowing along the PNG coast in the Bismarck Sea (red streamfunctions of Figure 3c), only the removal flux was significant, varying between 2.3 and 2.5 t(Nd) yr^{-1}. Therefore, scavenging of dissolved Nd prevailed over PNG margin inputs (section 3.2.1). Comparing the F_{net} along this pathway (-1.9 t(Nd) yr^{-1}) to the net and total value determined by the equation (1) (-3.0 t(Nd) yr^{-1}) revealed that the minor sources would also be dominated by scavenging along their transit prior to station 28 (blue and green streamfunctions of Figure 3c). Using equation (2), we quantified total $F_{ex,tot} = [0.9; 1.8]$ t(Nd) yr^{-1} and $F_{sc,tot} = [3.9; 4.8]$ t(Nd) yr^{-1}, the smallest value referring to $\varepsilon_{sc} = \varepsilon_i$ and the largest one to $\varepsilon_{sc} = \varepsilon_f$ (Figure 5b).

Contrastingly, dominant Nd supply fluxes were found for the CW, mainly associated to the water masses following the major pathway (red streamfunctions in Figure 4c; $F_{ex} = [4.8; 5.6]$ t(Nd) yr^{-1} and $F_{sc} = [2.1-2.8]$ t(Nd) yr^{-1}, the smallest values being again associated to $\varepsilon_{sc} = \varepsilon_i$). Balanced and smallest fluxes were

quantified along the minor pathways, leading to total fluxes equal to $F_{ex,tot}$ = [5.8; 6.9] t(Nd) yr^{-1} and $F_{sc,tot}$ = [3.2; 4.3] t(Nd) yr^{-1} (Figure 5b). Although supplies of Nd dominate along this water trajectory, both calculated fluxes of Nd supply and removal were significant.

3.2.3. Supply and Scavenging Fluxes Qualified for Water Masses Constituting the Solomon Sea Thermocline (Flu-22 TW and Flu-22 CW Experiments)

Regarding the Flu-22 TW and Flu-22 CW experiments, no pathway was sufficiently dominant to allow us to make a similar assumption. The underdetermined system of two equations and four unknowns (F_{ex}, F'_{ex}, F_{sc}, F'_{sc}) led us to use different hypotheses that resulted in less robust estimates of the fluxes. The tested hypotheses are summarized in Appendix A (see text and Figure A1), as well as the flux quantifications resulting from these different hypotheses (Figure A2). Without going into details, hypotheses are about the location of the scavenging, and the assumption that all the geochemical enrichments are occurring along one of the two pathways. We then tested the sensitivity of our results to these hypotheses. For each hypothesis, we obtained a range of values for $F_{ex,tot}$ and $F_{sc,tot}$ and we considered the most extreme values to define the final range within which $F_{ex,tot}$ and $F_{sc,tot}$ are expressed in Figure 5b. To be cautious and not overinterpret these estimations, we only present, for each layer, the flux that seems to most significantly influence the $F_{net,tot}$.

It is interesting to note that, along the transit of the SS-TW, whichever the assumption made, the flux estimates for $F_{ex,tot}$ and $F_{sc,tot}$ are very similar, giving us confidence in our results (Figures 5b and A2). The positive $F_{net,tot}$ is mainly explained by a significant $F_{ex,tot}$ around 2.6 t(Nd) yr^{-1} meaning that the waters seem to be mostly affected by Nd supplies along their pathways. The scavenging along these pathways must be much smaller, around 0.7 t(Nd) yr^{-1}.

On the contrary, the fluxes estimated along the transit of the SS-CW are very variable depending on the different hypotheses, mostly reflecting the lack of Nd data to constrain the water masses and sources. Added to the transport underestimation of the modeled NVJ-CW, this precluded any clear conclusion about the intensity of the fluxes yielding the negative $F_{net,tot}$ (see Figure A2): we are not able to say whether the negative $F_{net,tot}$ resulted from both significant Nd supply and removal fluxes, or only from Nd removal along their pathways.

3.2.4. Strategy Suggested for Future Study Based on This Coupled Approach of Virtual/Real Tracer

The limitations encountered in this study, mainly due to its pioneer nature, lead us to propose a strategy to improve the exchange flux calculations, and more generally to conduct geochemical data acquisition.

The Lagrangian analyses coupled to OGCM outputs should be performed before the preparation of the sampling cruise plans, because it would be beneficial for defining sampling strategy. For a considered water mass, its source locations and properties should be assessed with an appropriate model, as well as its pathways and the potential horizontal and vertical mixing that would occur. These characterizations would result in a better strategy for sampling the targeted water mass.

Then, the sampling strategy could target key locations—sources; upstream and downstream from mixing zones; along the margins—as illustrated in Figure 6 and detailed in its caption.

The robustness of the exchange flux calculations also depends on the spatial scale of the study area, the complexity of the water mass circulation and the evolution of its geochemical content. The more regional the scale is, the more constrained are the calculations and the more precise are the flux quantifications. The improvement of the characterization of exchange processes, in terms of fluxes, kinetics, and nature, seems to rest on relatively regional or local scale studies.

4. Discussion and Conclusions

This original coupled approach, using simulations from a realistic OGCM and in situ Nd data, allowed us to characterize the subduction areas, pathways and transports of the southwestern tropical Pacific thermocline waters and to refine—at different degrees depending on the water masses—the neodymium (Nd) fluxes experienced by these waters along their routes.
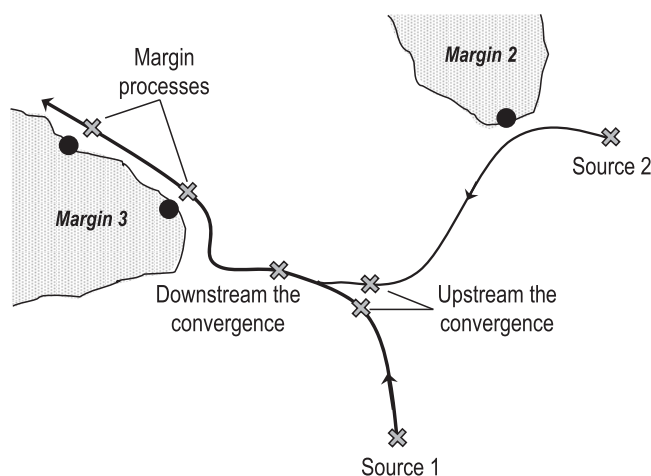
An important result is that the upper thermocline (Tropical Waters; TW) and lower thermocline (Central Waters; CW) waters have different subduction zones, pathways and geochemical enrichments as they flow from the southern subtropics to the equator, into the Coral Sea and out of the Solomon Sea.

At the southern entrance of the Solomon Sea, the Solomon Sea Tropical Waters (SS-TW) predominantly originate from the shallow North Vanuatu Jet (52%), which previously subducted between 130°W and 90°W, just north of station GYR. On the other hand, the denser Solomon Sea Central Waters (SS-CW) predominantly originate from the North Caledonian Jet (42%), which extends deeper, and originally subducted northeast of New Zealand, confirming the analyses of *Tsuchiya* [1981], *Tsuchiya et al.* [1989], and *Qu et al.* [2009] (Figures 3b and 4b and Table 1). These results agree with the vertical tilt of the poleward and equatorward redistribution of Coral Sea waters

Figure 6. Schematic description of key samples (gray crosses) needed to better constrain and estimate Nd exchange fluxes occurring along water mass pathways (black lines), suggested on the basis of the limitations encountered in this study. The water masses should be sampled at their source and upstream from any convergence, to avoid underdetermined system and, thus, allow a calculation that only includes one water mass, for each source. To verify the robustness of the relative contributions of water mass sources calculated through the Lagrangian experiments, a sample should be collected downstream from any convergence, to compare its parameters with those of the « upstream convergence » samples. Finally, at least two samples should be collected as a water mass begins and finishes to flow past a margin, to better constrain the exchange processes, their quantifications and their kinetics. The boundary exchange quantification implies also to constrain as precisely as possible the potential sedimentary sources of Nd. For that purpose, sediment samples should be collected to characterize the margins along which the water masses flow (black circles).

[*Kessler and Cravatte*, 2013]: Tropical Waters transiting via the North Caledonian Jet (NCJ-TW) mostly bifurcate southward at the Australian coast, whereas denser waters (NCJ-CW) mostly bifurcate northward toward the Solomon Sea.

This difference of predominant origin between the Solomon Sea TW and CW implies different pathways and different geochemical content evolutions. The upstream Nd exchanges differ between the upper and lower thermocline waters entering the Solomon Sea. The net Nd enrichment of the upper thermocline (SS-TW) likely results from external inputs supplied along its transit (Figure 5b). The ε_{Nd} values of rocks and sediments constituting the south tropical Pacific compiled in *Grenier et al.* [2013, Figure 12a] indicate that waters entering the southern Solomon Sea via the North Vanuatu Jet, representing more than 50% of the SS-TW, flow past more radiogenic areas than those entering via the North Caledonian Jet. This suggests that French Polynesia, Samoa and Vanuatu could be the major contributors to this Nd input (Figure 3b). Contrasting with the Tropical Waters, Central Waters seem to undergo strong net scavenging—although this value could be underestimated—before entering the Solomon Sea ($F_{net,tot} = -1.6 \pm 0.5$ t(Nd) yr^{-1}, Figure 5b), specifically along the Australian coast, although we could not determine the strength of each exchange flux (see section 3.2.3). Better documentation of the Nd fluxes in the southwestern Pacific waters should be obtained from new PANDORA cruise results (GEOTRACES section GP12, July 2012) [*Eldin et al.*, 2013]. The unfortunate lack of Nd data in the vicinity and north of New Zealand, in the subduction zone of CW, prevented us from computing geochemical fluxes for the CW upstream from their entrance into the Coral Sea.

Within the Bismarck Sea, the TW are rather depleted in their Nd content (28 TW; Figures 3c and 5b). Scavenging of Nd from the TW may occur as it is conveyed by the NGCU past the narrow and steep canyon characterizing the mouth surroundings of the Sepik River. Indeed, the large outflow of particulate matter and the uneven bathymetry result in high particle concentration layers—called Intermediate Nepheloid Layers—that could readily adsorb Nd [*Kineke et al.*, 2000]. The strong scavenging potential of sediment resuspension deposited in the delta of some passive margins for particle reactive elements such as Nd could also be hypothesized as an explanation for this high Nd scavenging [*Kuehl et al.*, 2004]. Contrasting

with the upper layer, the deeper CW of the Bismarck Sea (28 CW) exhibited the strongest dissolved Nd enrichment among the thermocline waters studied here (Figure 5b). This result confirms previous suggestions about the crucial role of the Papua New Guinea margins for the geochemical enrichment of the equatorial cold tongue [*Lacan and Jeandel*, 2001; *Slemons et al.*, 2010; *Radic et al.*, 2011; *Grenier et al.*, 2013]. The CW flowing along Papua New Guinea coast near station 28 are the only waters where both $F_{ex,tot}$ and $F_{sc,tot}$ are clearly significant, besides relatively high, suggesting that the Papua New Guinea coast of the Bismarck Sea is an important area for boundary exchange, at least at this density level (Figure 5b). One weakness of these flux quantifications is the lack of Nd concentrations at station 29, which forced us to estimate them from station SA-7 of *Zhang and Nozaki* [1996]. Fortunately, the thermocline waters flowing through Vitiaz Strait and St. George's Channel will be soon documented by new Nd data from the PANDORA cruise. They will allow us to verify whether our concentration estimations at station 29 are consistent or not and, thus, to validate the high variability and complexity of the geochemical processes that seem to occur at small vertical scales in the ocean.

Another way to assess the hypothesis that boundary exchange processes are enhanced along the PNG coasts in the Bismarck Sea, in the vicinity of the Sepik River mouth, is to compare the flux of sedimentary Nd discharged by the Sepik River on the shelf/slope and transported offshore, to the flux of dissolved Nd transported within the thermocline waters. *Kuehl et al.* [2004] estimated that, of the total sediment discharged by the Sepik River ($\sim$80 Mt yr^{-1}) [*Chappell*, 1993], only $\sim$10% accumulates on the adjacent shelf and slope. The remaining amount presumably escapes offshore via gravity flows—called hyperpycnals—through a submarine canyon ($\sim$72 Mt yr^{-1} of sediments). The mean concentration of Nd measured in the sediment and rocks of the Bismarck Sea area is 16 ppm (extracted from the EarthChem database) [*Grenier et al.*, 2013, region n°2 of Figure 12a]. Therefore, the flux of sedimentary Nd associated to the Sepik River discharge is estimated to 130 t(Nd) yr^{-1} accumulated on the shelf and slope and 1150 t(Nd) yr^{-1} transported offshore by the hyperpycnals. The dissolved Nd flux transported by the thermocline waters in this area is deduced from the simulated transports for the TW and the CW along the PNG coasts and their mean dissolved Nd concentrations (3.0 pmol kg^{-1} for the TW, 5.0 pmol kg^{-1} for the CW). The resulting fluxes of dissolved Nd are estimated to be 30 t(Nd) yr^{-1} for the TW and 80 t(Nd) yr^{-1} for the CW, for a total of 110 t(Nd) yr^{-1}. Comparison of solid and dissolved Nd fluxes yields to elevated particulate/dissolved ratios: roughly 1/1 for the waters flowing along the shelf and slope and up to 10/1 for the waters potentially crossing the hyperpycnal. These are upper limits because we only consider the flux of dissolved Nd of the thermocline waters and not of the entire water column, a huge part of the water column transport being associated to the thermocline waters in this area [*Cravatte et al.*, 2011; *Grenier et al.*, 2011]. These particulate Nd fractions are very high in comparison to those measured in the open ocean ($\sim$5%) [*Bertram and Elderfield*, 1993; *Jeandel et al.*, 1995]. Such high ratios could support strong exchange between the sedimentary Nd of the PNG margins and dissolved Nd in the water column. These important exchange fluxes occur in less than a month, which is the mean residence time estimated for the CW between stations 29 and 28, suggesting that sediment/water interactions are characterized by rapid kinetics. This time scale is consistent with recent experimental results which showed that Nd can be released from riverine or shelf basaltic sediments on weekly time scales [*Pearce et al.*, 2013]. This study also showed that a fraction of this released Nd can be subsequently removed from the solution because of secondary-phase precipitation. Thus, experimental results confirmed that particle/solution exchange can occur on time scales consistent with our field observations.

The opposite F_{net} found between the upper and lower thermocline waters flowing along the PNG coasts (Figure 5b) is consistent with the fact that dissolved iron (Fe) maximum is found only in the lower thermocline [*Slemons et al.*, 2010; *Radic et al.*, 2011] whereas the particulate Fe maximum is found in the upper thermocline, along the equator [*Slemons et al.*, 2012, Figure 5]. These results suggest that a larger export of sedimentary particles may occur within the TW than within the CW. These opposite values of F_{net} reflect the complexity of the relationship between the water transport and its geochemical enrichment. In our area at least, the bathymetry, the particulate activity, and the river discharge might strongly impact the geochemical content of the water masses.

As a conclusion, the southwestern tropical Pacific is identified as a major player in the climate regulation for both dynamical and geochemical reasons: (1) a substantial amount of water formed in the South Pacific subtropical gyre transits through the Coral and Solomon seas before joining the Equatorial Undercurrent

(EUC) and upwelling in the equatorial cold tongue and (2) the EUC likely gains much of its geochemical fingerprint from the copious sediment-loaded runoff from PNG and the surrounding tropical islands, although this needs to be quantified. The coupling between high-resolution physical modeling, Lagrangian approach and geochemical tracers proposed here is a novel approach. The water transport quantification from model outputs allows refined flux estimates, crucial for calculating the most realistic dissolution rates yielding the calculated Nd release. Understanding under which conditions and at which rates tracers are introduced in (or removed from) the ocean is of first importance to constrain and model the element cycles. The present work, conducted on a small geographical scale and based on a refined modeled circulation, allows distinguishing areas where inputs seem to dominate whereas others are submitted to strong scavenging, which was not expected before [*Johnson et al.*, 1999; *Lacan and Jeandel*, 2001; *Mackey et al.*, 2002]. Mostly, the impact of a copious sediment-loaded river discharge is better understood after this work. Clearly, the limiting factor here is the small number of Nd concentration measurements, which often lead us to make approximations and assign to some stations concentration values measured at other stations. Also, one should not forget that an important difference between the virtual and the real tracer approaches is the time scale difference: each geochemical measurement represents synoptic data and, in our study, the measurements used for the calculations come from samples collected during different cruises, realized during different seasons (austral spring and summer) and years (different El Niño – Southern Oscillation states), which means different atmospheric and oceanic conditions; by contrast, the water mass transports are simulated from OGCM outputs that are integrated over years and, consequently, smooth the temporal variability of the transports. To reduce this time scale difference, it would be ideal to occupy the geochemical stations in different seasons and years to assess the geochemical variability and then to define mean values. So far, the temporal variability of trace elements in the ocean is still poorly known and its assessment is a very difficult task to carry out considering the resources needed to get data. GEOTRACES will hopefully reduce the gap between physical and geochemical samples. This will help improving our knowledge of the land-to-ocean fluxes, an urgent task.

Appendix A

A1. Assumptions Made to Estimate Export and Scavenging Fluxes of Flu-22 TW (SS-TW) and Flu-22 CW (SS-CW)

For experiments Flu-22 TW and Flu-22 CW, in order to have an estimate of both total supply ($F_{ex,tot}$) and scavenging flux ($F_{sc,tot}$) from which results $F_{net,tot}$, we made different assumptions, fixing different parameters of equation (2), which allowed us to estimate the different unknowns. Then, we assessed their sensitivity by varying different parameters. The approach followed for the different assumptions is summarized in Figure A1 and detailed below.

1. Hypothesis A: We made the assumption of independent contributions, meaning that each trajectory constituting the final thermocline water contributes alone to the ε_{Nd} and Nd concentration changes. Under this assumption, the two-equation system becomes:

$$
\begin{cases}
W \cdot [Nd]_f = W \cdot [Nd]_i + F_{ex} - F_{sc} & \text{(A1)} \\
W \cdot \varepsilon_f \cdot [Nd]_f = W \cdot \varepsilon_i \cdot [Nd]_i + F_{ex} \cdot \varepsilon_{ex} - F_{sc} \cdot \varepsilon_{sc} & \text{(A2)} \\
W' \cdot [Nd]_f = W' \cdot [Nd]_i' + F_{ex}' - F_{sc}' & \text{(A3)} \\
W' \cdot \varepsilon_f \cdot [Nd]_f = W' \cdot \varepsilon_i' \cdot [Nd]_i' + F_{ex}' \cdot \varepsilon_{ex}' - F_{sc}' \cdot \varepsilon_{sc}' & \text{(A4)}
\end{cases}
$$

1.1. Hypotheses A_i and A_f: In this first case of independent contribution assumption, we calculate the four fluxes F_{ex}, F_{ex}', F_{sc}, and F_{sc}' for the extreme values that can be assigned to ε_{sc} and ε_{sc}'. Note that defining ε_{sc}—the isotopic signature of the water mass during scavenging process—is required for the calculation of $F_{ex,tot}$ and $F_{sc,tot}$. In a realistic ocean, ε_{sc} is a combination of ε_i and ε_f. However, this combination cannot be determined in case of off-line inverse calculation. Previous studies assigned the final ε_f value to the scavenging fluxes, making the assumption of a homogenized water mass within the box [e.g., *Lacan and Jeandel*, 2005]. To assess the impact of this hypothesis on the flux estimates and their sensitivity to this parameter, we performed two flux calculations: (i) one considering $\varepsilon_{sc} = \varepsilon_i$, which supposes that scavenging occurs just
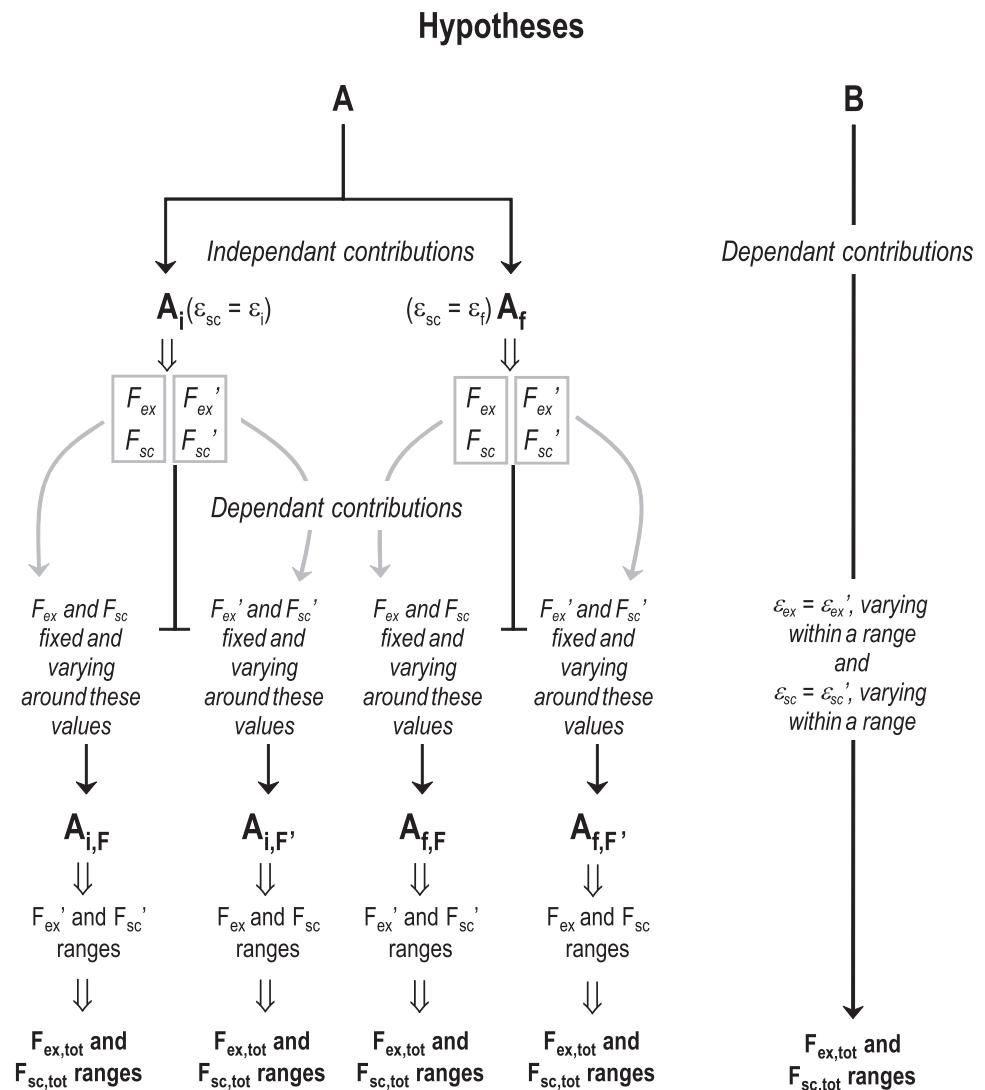
Figure A1. Schematic description of the different hypotheses A—subdivided in $A_{i,F}$, $A_{i,F'}$, $A_{f,F}$, $A_{f,F'}$—and B defined to estimate the total exchange fluxes $F_{ex,tot}$ and $F_{sc,tot}$ from which results $F_{net,tot}$.

downstream of station 29 location (see red segment in Figures 3c and 4c); (ii) the other considering $\varepsilon_{sc} = \varepsilon_f$, which supposes that scavenging occurs just at station 28 (see black point in Figures 3c and 4c). The "true" value should be found between these two values.

-Hypothesis A_i: The scavenging fluxes occur at the beginning of the trajectories and each scavenging flux is assigned to the initial isotopic compositions, i.e., $\varepsilon_{sc} = \varepsilon_i$ and $\varepsilon_{sc}' = \varepsilon_i'$,

-Hypothesis A_f: The scavenging fluxes occur at the end of the trajectories and each scavenging flux is assigned to the final isotopic composition, i.e., $\varepsilon_{sc} = \varepsilon_{sc}' = \varepsilon_f$.

We are aware of how strong is the hypothesis of independent contribution; we only use these calculations as preliminary results to estimate the range of values within which these fluxes likely are.

1.2. Hypotheses $A_{i,F}$, $A_{i,F'}$, $A_{f,F}$, and $A_{f,F'}$: We now consider dependent contributions of the initial Nd parameters of the water masses to the ε_{Nd} and Nd concentration changes.

-Hypothesis $A_{i,F}$: Considering $\varepsilon_{sc} = \varepsilon_i$ and $\varepsilon_{sc}' = \varepsilon_i'$, we make F_{ex} and F_{sc} vary around the value we found previously and calculate F_{ex}' and F_{sc}'.

a)

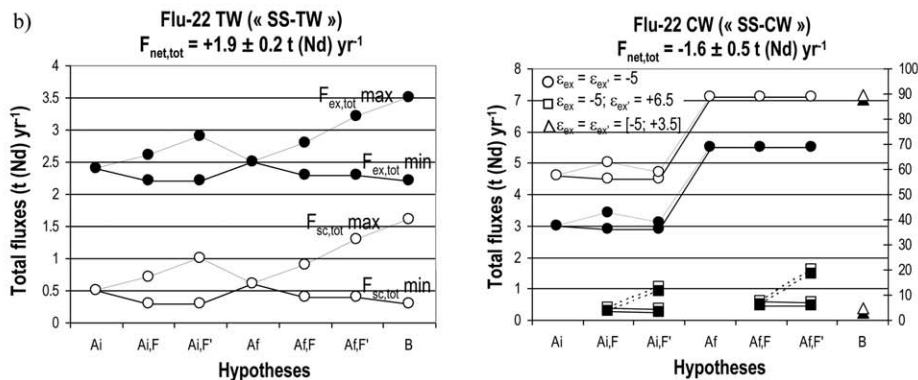|	Pathway	A_i	$A_{i,F}$	$A_{i,F'}$	A_f	$A_{f,F}$	$A_{f,F'}$	B	Data source and informations
Flu-22 TW (« SS-TW »)	Source ε_i: Flu-43	$\varepsilon_{ex} = +4.1$ $\varepsilon_{ex}' = +6.5$	$\varepsilon_{ex} = +4.1$ $\varepsilon_{ex}' = +6.5$	$\varepsilon_{ex} = +4.1$ $\varepsilon_{ex}' = +6.5$	$\varepsilon_{ex} = +4.1$ $\varepsilon_{ex}' = +6.5$	$\varepsilon_{ex} = +4.1$ $\varepsilon_{ex}' = +6.5$	$\varepsilon_{ex} = +4.1$ $\varepsilon_{ex}' = +6.5$	$\varepsilon_{ex} = \varepsilon_{ex}' =$ [+4.1; +6.5]	Mean ε_{Nd} values of samples of rocks and sediments of areas 3 and 7 of Grenier et al. (2013), extracted from the geochemical data set EarthChem
	Source ε_i': GYR								
Flu-22 CW (« SS-CW »)	Source ε_i: Flu-43	$\varepsilon_{ex} = \varepsilon_{ex}' = -5.0$	$\varepsilon_{ex} = \varepsilon_{ex}' = -5.0$	$\varepsilon_{ex} = \varepsilon_{ex}' = -5.0$	$\varepsilon_{ex} = \varepsilon_{ex}' = -5.0$	$\varepsilon_{ex} = \varepsilon_{ex}' = -5.0$	$\varepsilon_{ex} = \varepsilon_{ex}' = -5.0$	$\varepsilon_{ex} = \varepsilon_{ex}' =$ [-5.0; -3.5]	- $\varepsilon_{Nd} = -5.0$: measured on sediment samples collected in the Gulf of Papua. - $\varepsilon_{Nd} = +6.5$: mean ε_{Nd} values of samples of rocks and sediments of area 7 of Grenier et al. (2013), extracted from the geochemical data set EarthChem - Hyp B: Resolution cannot be made within the range [-5.0; +6.5] since mathematically, formulae cannot be resolved for values greater than -3.5
	Source ε_i': GYR	$\varepsilon_{ex} = -5.0$ $\varepsilon_{ex}' = +6.5$	$\varepsilon_{ex} = -5.0$ $\varepsilon_{ex}' = +6.5$	$\varepsilon_{ex} = -5.0$ $\varepsilon_{ex}' = +6.5$	$\varepsilon_{ex} = -5.0$ $\varepsilon_{ex}' = +6.5$	$\varepsilon_{ex} = -5.0$ $\varepsilon_{ex}' = +6.5$	$\varepsilon_{ex} = -5.0$ $\varepsilon_{ex}' = +6.5$		

b)

Figure A2. (a) Definition of the ε_{ex} and ε_{ex}' values or ranges chosen for the calculation of the exchange fluxes, following the different hypotheses A and B. ε_{ex} and ε_{ex}' values are defined following the ε_{Nd} data available via direct measurements of sediment samples or via the geological database EarthChem (see « Data source and information » column). The choice of these values is constrained by the necessity to obtain positive resulting fluxes (unless net fluxes that can be positive or negative). (b) Calculated total fluxes $F_{ex,tot}$ (black symbols) and $F_{sc,tot}$ (white symbols), in tons of Nd per year, following the different assumptions made (hypotheses A_i, $A_{i,F}$, $A_{i,F'}$, A_f, $A_{f,F}$, $A_{f,F'}$ and B) for (left) Flu-22 TW and (right) Flu-22 CW. The total net flux is reported below the name of each considered water mass. For each hypothesis where we make vary flux values (A_i, $A_{i,F'}$, $A_{f,F}$, and $A_{i,F'}$) or ε_{ex} and ε_{sc} values (hypothesis B), we report the minimum (continuous line) and maximum (dashed line) value of the total flux obtained. The difference between the $F_{ex,tot}$ maximum and the $F_{sc,tot}$ maximum and between the $F_{ex,tot}$ minimum and the $F_{sc,tot}$ minimum is constant, equal to $F_{net,tot}$. For CW, we identify by different symbols the calculations made for different choices of ε_{ex} and ε_{ex}' values (see Figure A2a). No data are reported for the CW, under hypotheses A_i and A_f, for the choice of ε_{ex} and ε_{ex}' values assigned to the squares because the resulting fluxes are negative. The larger flux scale on the right side of the graph associated to Flu-22 CW total fluxes is associated with the choices of ε_{ex} and ε_{ex}' values represented by squares and by triangles.

-Hypothesis $A_{i,F'}$: Considering $\varepsilon_{sc} = \varepsilon_i$ and $\varepsilon_{sc}' = \varepsilon_i'$, we make F_{ex}' and F_{sc}' vary around the value we found previously and calculate F_{ex} and F_{sc}.

-Hypothesis $A_{f,F}$: Considering $\varepsilon_{sc} = \varepsilon_{sc}' = \varepsilon_f$, we make F_{ex} and F_{sc} vary around the value we found previously and calculate F_{ex}' and F_{sc}'.

-Hypothesis $A_{f,F'}$: Considering $\varepsilon_{sc} = \varepsilon_{sc}' = \varepsilon_f$, we make F_{ex}' and F_{sc}' vary around the value we found previously and calculate F_{ex} and F_{sc}.

ε_{ex} values are fixed following the available ε_{Nd} data of sediments we get via direct measurements or via the geological database EarthChem (http://www.earthchem.org).

2. Hypothesis B: We consider the dependence of each water mass contribution to the ε_{Nd} and Nd concentration changes and we test the flux sensitivity to ε_{Nd} values assigned to F_{ex} and F_{ex}' along the water mass pathways. To free ourselves from the underdetermination of the equation system, we assume that $\varepsilon_{ex} = \varepsilon_{ex}'$ and $\varepsilon_{sc} = \varepsilon_{sc}'$. Under this assumption, we are now able to determine total fluxes $F_{ex,tot}$ and $F_{sc,tot}$, which will be compared to the total fluxes $F_{ex,tot}$ and $F_{sc,tot}$, determined in hypothesis A (Figure A1). To test the sensitivity of these fluxes to the ε_{ex} and ε_{sc} values, we make ε_{ex} and ε_{sc} vary between a likeable range of value. ε_{sc} values range between ε_i, ε_i', and ε_f values. ε_{ex} values range between the values defined for ε_{ex} and ε_{ex}' in hypothesis A.

The total supply and scavenging fluxes obtained for each experiment Flu-22 TW and Flu-22 CW under the different hypotheses are represented in Figure A1.

References

Barnier, B., et al. (2006), Impact of partial steps and momentum advection schemes in a global ocean circulation model at eddy permitting resolution, *Ocean Dyn.*, *56*, 543–567, doi:10.1007/s10236-006-0082-1.

Bertram, C. J., and H. Elderfield (1993), The geochemical balance of the Rare Earth Elements and Nd isotopes in the oceans, *Geochim. Cosmochim. Acta*, *57*, 1957–1986.

Blanke, B., and P. Delecluse (1993), Variability of the tropical Atlantic Ocean simulated by a general circulation model with two different mixed-layer physics, *J. Phys. Oceanogr.*, *23*, 1363–1388.

Blanke, B., and S. Raynaud (1997), Kinematics of the Pacific Equatorial Undercurrent: An Eulerian and Lagrangian approach from GCM results, *J. Phys. Oceanogr.*, *27*, 1038–1053.

Blanke, B., M. Arhan, G. Madec, and S. Roche (1999), Warm water paths in the equatorial Atlantic as diagnosed with a general circulation model, *J. Phys. Oceanogr.*, *29*, 2753–2768.

Chappell, J. (1993), Contrasting Holocene sedimentary geologies of lower Daly River, northern Australia, and lower Sepik–Ramu, Papua New Guinea, *Sediment. Geol.*, *83*, 339–358.

Cravatte, S., A. Ganachaud, Q.-P. Duong, W. S. Kessler, G. Eldin, and P. Dutrieux (2011), Observed circulation in the Solomon Sea from SADCP data, *Prog. Oceanogr.*, *88*, 116–130.

Eldin, G., A. Ganachaud, S. Cravatte, and C. Jeandel (2013), Pandora cruise provides an unprecedented description of the Solomon Sea, *CLIVAR Exch.*, *18*(61), 24–25.

Fine, R. A., R. Lukas, F. Bingham, M. J. Warnar, and R. H. Gammon (1994), The western equatorial Pacific: A water mass crossroads, *J. Geophys. Res.*, *99*, 25,063–25,080.

Gasparin, F., A. Ganachaud, and C. Maes (2011), A western boundary current east of New Caledonia: Observed characteristics, *Deep Sea Res., Part I*, *58*, 956–969.

Gasparin, F., A. Ganachaud, C. Maes, F. Marin, and G. Eldin (2012), Oceanic transports through the Solomon Sea: The bend of the New Guinea Coastal Undercurrent, *Geophys. Res. Lett.*, *39*, L15608, doi:10.1029/2012GL052575.

Gourdeau, L., W. Kessler, R. Davis, J. Sherman, C. Maes, and E. Kestenare (2008), Zonal jets entering the Coral Sea, *J. Phys. Oceanogr.*, *38*, 715–725.

Grenier, M., S. Cravatte, B. Blanke, C. Menkes, A. Koch-Larrouy, F. Durand, A. Melet, and C. Jeandel (2011), From the western boundary currents to the Pacific Equatorial Undercurrent: Modeled pathways and water mass evolutions, *J. Geophys. Res.*, *116*, C12044, doi:10.1029/2011JC007477.

Grenier, M., C. Jeandel, F. Lacan, D. Vance, C. Venchiarutti, A. Cros, and S. Cravatte (2013), From the subtropics to the central equatorial Pacific Ocean: Neodymium isotopic composition and Rare Earth Element concentration variations, *J. Geophys. Res.*, *118*, 1–27, doi: 10.1029/2012JC8239.

Jeandel, C., J. K. Bishop, and A. Zindler (1995), Exchange of Nd and its isotopes between seawater small and large particles in the Sargasso Sea, *Geochim. Cosmochim. Acta*, *59*, 535–547.

Jeandel, C., B. Peucker-Ehrenbrink, M. T. Jones, C. R. Pearce, E. H. Oelkers, Y. Godderis, F. Lacan, O. Aumont, and T. Arsouze (2011), Ocean margins: The Missing term in oceanic element budgets, *Eos Trans. AGU*, *92*(26), 217–218.

Jeandel, C., H. Delattre, M. Grenier, C. Pradoux, and F. Lacan (2013), Rare earth concentrations and Nd isotopes in the South East Pacific Ocean, *Geochem. Geophys. Geosyst.*, *14*, 328–341, doi:10.1029/2012GC004309.

Johnson, K. S., F. P. Chavez, and G. E. Friederich (1999), Continental shelf sediment as a primary source of iron for coastal phytoplankton, *Nature*, *398*, 697–700.

Jones, M. T., C. R. Pearce, and E. H. Oelkers (2012), An experimental study of the interaction of basaltic riverine particulate material and seawater, *Geochim. Cosmochim. Acta*, *77*, 108–120, doi:10.1016/j.gca.2011.10.044.

Kessler, W. S. (1999), Interannual variability in the subsurface high-salinity tongue south of the equator at 165°E, *J. Phys. Oceanogr.*, *29*, 2038–2049.

Kessler, W. S., and S. Cravatte (2013), Mean circulation of the Coral Sea, *J. Geophys. Res.*, *118*, 6385–6410, doi:10.1002/2013JC009117.

Kineke, G. C., K. J. Woolfe, S. A. Huehl, J. D. Milliman, T. M. Dellapenna, and R. G. Purdon (2000), Sediment export from the Sepik River, Papua New Guinea: Evidence for a divergent sediment plume, *Cont. Shelf Res.*, *20*, 2239–2266.

Kuehl, S. A., G. J. Brunskill, K. Burns, D. Fugate, T. Kniskern, and L. Meneghini (2004), Nature of sediment dispersal off the Sepik River, Papua New Guinea: Preliminary sediment budget and implications for margin processes, *Cont. Shelf Res.*, *24*, 2417–2429.

Lacan, F., and C. Jeandel (2001), Tracing *Papua* New Guinea imprint on the central Equatorial Pacific Ocean using neodymium isotopic compositions and Rare Earth Element patterns, *Earth Planet. Sci. Lett.*, *186*, 497–512.

Lacan, F., and C. Jeandel (2005), Neodymium isotopes as a new tool for quantifying exchange fluxes at the continent–ocean interface, *Earth Planet. Sci. Lett.*, *232*(3–4), 245–257, doi:10.1016/j.epsl.2005.01.004.

Levitus, S., T. Boyer, M. Conkright, D. Johnson, T. O'Brien, J. Antonov, C. Stephens, and R. Gelfeld (1998), Introduction, in *World Ocean Database 1998, NOAA Atlas NESDIS 18*, vol.1, 346 pp., U.S. Govt. Print. Off., Washington, D. C.

Mackey, D. J., J. E. O'Sullivan, and R. J. Watson (2002), Iron in the western Pacific: A riverine or hydrothermal source for iron in the Equatorial Undercurrent, *Deep Sea Res., Part I*, *49*, 877–893.

Madec, G. (2008), *NEMO Ocean Engine. Note du Pole de Modélisation 27*, 300 pp., Inst. Pierre-Simon Laplace, France.

Melet, A., L. Gourdeau, W. S. Kessler, J. Verron, and J.-M. Molines (2010), Thermocline circulation in the Solomon Sea: A modeling study, *J. Phys. Oceanogr.*, *40*, 1302–1319.

Melet, A., J. Verron, L. Gourdeau, and A. Koch-Larrouy (2011), Equatorward pathways of Solomon Sea water masses and their modifications, *J. Phys. Oceanogr.*, *41*, 810–826, doi:10.1175/2010JPO4559.1.

Montgomery, R. B. (1937), A suggested method for representing gradient flow in isentropic surfaces, *Bull. Am. Meteorol. Soc.*, *18*, 210–212.

Pearce, C. R., M. T. Jones, E. H. Oelkers, C. Jeandel, and C. Pradoux (2013), The importance of particulate dissolution for the marine neodymium (Nd) isotope and Rare Earth Element (REE) budgets, *Earth Planet. Sci. Lett.*, *369–370*, 138–147.

Piepgras, D. J., and G. J. Wasserburg (1987), Rare earth element transport in the western North Atlantic inferred from Nd isotopic observations, *Geochim. Cosmochim. Acta*, *51*, 1257–1271.

Qu, T., and E. J. Lindstrom (2002), A climatological interpretation of the circulation in the Western South Pacific, *J. Phys. Oceanogr.*, *32*(9), 2492–2508.

Qu, T., S. Gao, I. Fukumori, R. Fine, and E. J. Lindstrom (2009), Origin and pathway of equatorial 13°C water in the Pacific identified by a simulated passive tracer and its adjoint, *J. Phys. Oceanogr.*, *39*, 1836–1853.

Radic, A., F. Lacan, and J. W. Murray (2011), Isotopic composition of dissolved iron in the equatorial Pacific Ocean: New constraints for the oceanic iron cycle, *Earth Planet. Sci. Lett.*, *306*, 1–10, doi:10.1016/j.epsl.2011.03.015.

Ridgway, K. R., J. R. Dunn, and J. L. Wilkin (2002), Ocean interpolation by four-dimensional weighted least squares—Application to the waters around Australasia, *J. Atmos. Oceanic Technol.*, *19*, 1357–1375.

Rodgers, K. B., B. Blanke, G. Madec, O. Aumont, P. Ciais, and J.-C. Dutay (2003), Extratropical sources of Equatorial Pacific upwelling in an OGCM, *Geophys. Res. Lett.*, *30*(2), 1084, doi:10.1029/2002GL016003.

Roemmich, D., and B. Cornuelle (1992), The subtropical mode waters of the South Pacific Ocean, *J. Phys. Oceanogr.*, *22*, 1178–1187.

Ryan, J. P., I. Ueki, Y. Chao, H. Hang, P. S. Polito, and F. P. Chavez (2006), Western Pacific modulation of large phytoplankton blooms in the central and eastern equatorial Pacific, *J. Geophys. Res.*, *111*, G02013, doi:10.1029/2005JG000084.

Singh, S. P., S. K. Singh, V. Goswami, R. Bhushan, and V. K. Rai (2012), Spatial distribution of dissolved neodymium and ε_{Nd} in the Bay of Bengal: Role of particulate matter and mixing of water masses, *Geochim. Cosmochim. Acta*, *94*, 38–56.

Slemons, L. O., J. W. Murray, B. Paul, and P. Dutrieux (2010), Western Pacific coastal sources of iron, manganese and aluminium to the Equatorial Undercurrent, *Global Biogeochem. Cycles*, *24*, GB3024, doi:10.1029/2009GB003693.

Slemons, L. O., B. Paul, J. Resing, and J. W. Murray (2012), Particulate iron, aluminum and manganese in the Pacific equatorial undercurrent and low latitude western boundary current sources, *Mar. Chem.*, *142–144*, 54–67.

SPICE Community (2012), Naming a western boundary current from Australia to the Solomon Sea, *CLIVAR Newsl. Exch.*, *16*(56), 28.

Tomczak, M., and J. S. Godfrey (2003), *Hydrology of the Pacific Ocean, Regional Oceanography: An Introduction*, 2nd improved ed., pp. 137–156, Daya Publ. House, Delhi, India.

Tomczak, M., and D. Hao (1989), Water masses in the thermocline of the Coral Sea, *Deep Sea Res., Part A*, *36*(10), 1503–1514.

Tsuchiya, M. (1981), The origin of the Pacific equatorial 13°C water, *J. Phys. Oceanogr.*, *11*, 794–812.

Tsuchiya, M., R. Lukas, R. Fine, E. Firing, and E. Lindstrom (1989), Source waters of the Pacific Equatorial Undercurrent, *Prog. Oceanogr.*, *23*, 101–147.

Wasserburg, G. J., S. B. Jacobsen, D. L. De Paolo, M. T. McCulloch, and T. Wen (1981), Precise determination of Sm/Nd ratios, Sm and Nd isotopic abundances in standard solutions, *Geochim. Cosmochim. Acta*, *45*, 2311–2323.

Yeager, S. G., and W. G. Large (2004), Late-winter generation of spiciness on subducted isopycnals, *J. Phys. Oceanogr.*, *34*, 1528–1545.

Zhang, J., and Y. Nozaki (1996), Rare earth elements and yttrium in seawater: ICP-MS determinations in the East Caroline, Coral Sea and South Fiji basins of the western south Pacific Ocean, *Geochim. Cosmochim. Acta*, *60*, 4631–4644.